POLITECNICO DI TORINO
Repository ISTITUZIONALE

ThreePhase WaterRheostat Dump Loads in Hydropower Plants: Failure Analysis of a Flawed Retrofit

Original
ThreePhase WaterRheostat Dump Loads in Hydropower Plants: Failure Analysis of a Flawed Retrofit / Freschi, F., Badami, M., Tartaglia, M.. - In: IET RENEWABLE POWER GENERATION. - ISSN 1752-1416. - 20:1(2026). [10.1049/rpg2.70312]

Availability:
This version is available at: 11583/3013294 since: 2026-07-20T11:57:08Z

Publisher:
Wiley

Published
DOI:10.1049/rpg2.70312

Terms of use:

This article is made available under terms and conditions as specified in the corresponding bibliographic description in the repository

Publisher copyright

(Article begins on next page)

19 November 2026

Check for updates

IET Renewable Power Generation

WILEY

The Institution of Engineering and Technology

ORIGINAL RESEARCH OPEN ACCESS

Three-Phase Water-Rheostat Dump Loads in Hydropower Plants: Failure Analysis of a Flawed Retrofit

Fabio Freschi | Marco Badami | Michele Tartaglia

Department of Energy – Politecnico di Torino, Torino, Italy

Correspondence: Fabio Freschi (fabio.freschi@polito.it)

Received: 10 April 2026 | **Revised:** 6 June 2026 | **Accepted:** 26 June 2026

ABSTRACT

When hydraulic regulation and spillways are unavailable or insufficient, grid-connected hydropower plants may require electrical dissipation systems to absorb power during load rejection and abnormal operating conditions. This paper analyses a refurbishment of a three-phase water-rheostat dump load installed in a large hydropower plant on the Po River (Italy), where immersion-depth regulation was replaced by electrode-spacing regulation. Field tests at incremental voltage levels (1–5–10 kV) and three-dimensional stationary current simulations were used to reconstruct the causal chain from observed phenomena to root causes. The retrofit exhibits intrinsic criticalities: (i) strong nonlinearity between the control variable (electrode spacing) and dissipated power, which amplifies positioning errors; (ii) local dielectric overstress driven by electrode geometry, with simulated peak electric field exceeding the design limit by more than three times at rated voltage; and (iii) phase-to-phase discharge triggered by the overflow water paths, which place line-to-line voltage across adjacent tanks. The results show that, for large-scale applications, design validation must jointly consider thermal-resistivity coupling, field enhancement and hydraulic layout of overflow paths. Practical design implications are provided for refurbishment and specification of water-rheostat dump loads in hydropower contexts.

1 | Introduction

Hydropower plants are typically designed with multiple systems to regulate power production in response to variations in load or operating conditions. The primary method of regulation is hydraulic, implemented through flow control mechanisms such as wicket gates, guide vanes or nozzles, which modulate the water entering the turbine to match electrical demand. In parallel, most large-scale installations include spillways, dedicated structures that allow water to bypass the turbine entirely in order to prevent flooding and mitigate hydraulic transients such as water hammer during load rejection or emergency shutdowns [1–3]. While spillways are essential for ensuring hydraulic safety and the structural integrity of dam systems, they may not always be available, feasible or sufficient to manage the full range of power fluctuations. In such cases, alternative means of electrical regulation are required.

Among these alternatives, electrical regulation using resistive loads, commonly referred to as dump loads, ballast loads or rheostat-based dissipation systems, has played a notable role. From a system point of view, a dump load acts as a controllable sink of active power to absorb surplus generation and support safe operation during critical events [4]. These systems are designed to absorb excess electrical power by diverting it to controlled resistive elements. Originally developed and widely applied in standalone micro-hydropower schemes, dump loads provide an effective way to maintain a constant load on the generator. This prevents overspeed conditions during sudden load rejection, ensures stable frequency and avoids the need for expensive mechanical governors [5]. The dumped energy is typically dissipated as heat through water or air heating elements, although in some cases, it is repurposed for ancillary uses such as domestic heating or water preheating [6]. In larger plants, dump loads have also been explored as an auxiliary solution

This is an open access article under the terms of the Creative Commons Attribution License, which permits use, distribution and reproduction in any medium, provided the original work is properly cited.
© 2026 The Author(s). *IET Renewable Power Generation* published by John Wiley & Sons Ltd on behalf of The Institution of Engineering and Technology.

to absorb transient surges or reduce the reliance on spillways [7].

While their simplicity and reliability have made resistive dump loads attractive in small- and medium-scale off-grid systems, a few documented applications exist at larger scales. These include emergency braking resistors or dynamic dissipation systems installed to support transient response or to reduce overspeed in the event of grid disconnection [8]. However, such implementations remain relatively rare and are usually custom-designed for specific plant configurations.

Despite their practicality, dump loads are not without limitations. Chief among these is the inherent energy inefficiency: energy that cannot be consumed by the grid or users is unavoidably wasted as heat, which raises questions of long-term sustainability [9]. Moreover, the physical size and cost of the resistive elements grow rapidly with plant power, making scaling beyond a certain threshold technically challenging [10]. Lastly, regulation strategies based on electrode geometry or immersion depth must take into account the nonlinear behavior of the system, as well as environmental variables such as water resistivity, which vary seasonally and can severely affect dissipation capacity [5, 6].

This paper analyses a large-scale resistive dump-load systems installed in a grid-connected hydropower plant located along the Po River, in northern Italy. The plant was built in the late 1950s and equipped with four vertical-axis Kaplan turbine units. The hydraulic head ranges from 3.5 m to 11 m, with a maximum flow rate of 1000 m^3/s. Each turbine unit originally delivered about 12.5 MW. The turbines were refurbished in the late 1980s, increasing their rated power to 20 MW, with a runner diameter of 7.6 m and a rotational speed of 53.6 rpm (112 poles).

The original design included a dump-load system consisting of three-phase rheostats capable of dissipating between 7 and 15 MW at 10 kV. These rheostats used variable water levels inside tanks to regulate the electrode immersion length and, consequently, the equivalent resistance. This approach allowed smooth power dissipation with automatic matching to the generated active power. However, following the plant's repowering, the existing rheostats became inadequate. Several design iterations were attempted to increase performance, culminating in a refurbished configuration based on adjustable electrode spacing.

The refurbished configuration was implemented as an industrial retrofit intended for full-scale operation. During commissioning, however, the system exhibited critical behaviour that prevented reliable operation at the specified power levels. This makes the case relevant primarily as the analysis of a flawed retrofit under real plant conditions. Such cases are seldom documented in detail, although they can provide useful information for future projects because they expose the limits of simplified design assumptions when electrical, thermal, hydraulic and mechanical effects interact at full scale. The purpose of this paper is therefore to reconstruct the failure mechanisms of the refurbished dump-load system by combining field measurements, design information and three-dimensional electrical simulations. The main contribution is the analysis of a real full-scale case, from the observed commissioning phenomena to the underlying physical causes. The results are then used to extract practical design constraints and engineering recommendations for future refurbishments of large water-rheostat dump loads [11].

Specifically, the paper provides:

1. an experimental characterization of power and equivalent resistance versus electrode spacing at 1–5–10 kV, highlighting the role of thermal resistivity coupling;
2. a three-dimensional stationary current simulation of the full geometry, used to link measured trends to current-density concentration and field enhancement;
3. a quantitative assessment of dielectric stress at critical electrode features, showing peak field values that exceed the assumed design limit at rated voltage;
4. an explanation of phase-to-phase discharge risk caused by overflow paths, which can expose adjacent tanks to line-to-line voltage;
5. a synthesis of the main design constraints and possible engineering improvements for future refurbishments, including electrode geometry, hydraulic layout, thermal management, control sensitivity and validation margins under water-resistivity variability.

Although the refurbishment analysed in this paper did not achieve the specified performance, it enables a structured reconstruction of the failure mechanisms and highlights the risks of oversimplified assumptions when resistive dissipation systems are adapted to repowered units.

2 | Three-Phase Rheostat Configurations: Original System

2.1 | Description

The original dissipation systems consisted of four three-phase rheostats, each designed for operation at 10 kV and for a regulated dissipated power between 7 and 15 MW.

The rheostat consists essentially of a steel sheet casing, on which are arranged the mechanical control assemblies and feed-through insulators connected to the current-carrying conductors, above a support frame (see Figure 1). These electrodes, placed 120° apart (see Figure 2), are made of steel tube and galvanized to mitigate the effects of environmental exposure, such as oxidation and corrosion, that would otherwise alter the surface conductivity with time. Since the system operates in a wet environment, the feed-through insulators–positioned on the upper frame of the rheostat tank were designed for the rated voltage of 10 kV. The original system measured the instantaneous active power and adjusted the rheostat to obtain an electrical load equal to that value. Regulation was achieved by changing the water level in the tank through the opening and closing of the three floodgates on the container perimeter. The reference water level was set using the measured resistivity of the river water, obtained from a dedicated sample vessel placed alongside the main tank, together with a calibration that relates resistivity and water level to the equivalent resistance.

17521424, 2026, 1, Downloaded from https://ietresearch.onlinelibrary.wiley.com/doi/10.1049/rpg2.70312 by Fabio Freschi - Politecnico Di Torino Sist. Bibl Del Polit Di Torino , Wiley Online Library on [17/07/2026]. See the Terms and Conditions (https://onlinelibrary.wiley.com/terms-and-conditions) on Wiley Online Library for rules of use; OA articles are governed by the applicable Creative Commons License



FIGURE 1 | Original power dissipation system.

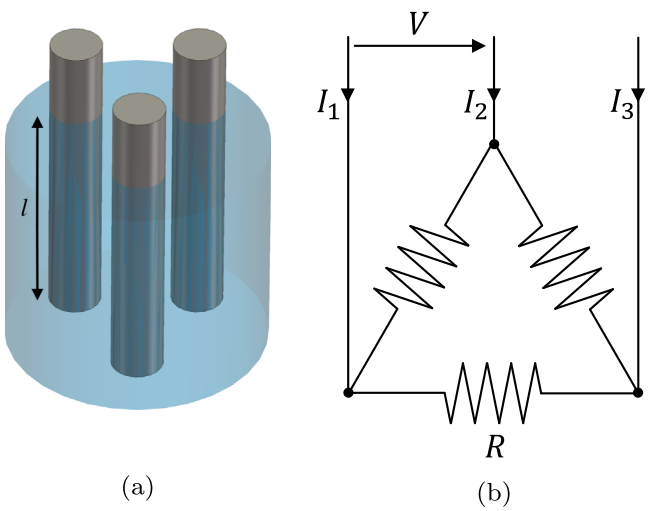


FIGURE 2 | (a) Sketch of the original dump-load system, (b) equivalent circuit

The water-level variation is achieved by the simultaneous operation of three floodgates arranged symmetrically with respect to the electrodes along the rheostat tank. The maximum level variation within the equipment is about 1.65 m. With such a level range, it is possible to adjust the power to be dissipated (for average values of water resistivity) between 10% and 100% of the nominal value. Overflow regulation is managed by a central gear motor unit connected by means of three rigid shafts to the control boxes of the operating screws. Water for the operation of the dissipator is supplied from below through an adductor pipe with a nominal diameter of 400 mm.

A preliminary setup defined the relationship between the water level and water resistivity with the equivalent resistance of the system. The dissipator is activated upon a request from the unit protection system, with the rheostat follower enabled. In follower operation, the drain flow rate is kept constant to avoid abrupt level changes. When the protection intervenes, the electrical network is disconnected and the rheostat is immediately connected to the generator. No-load conditions occur only in case of malfunction



FIGURE 3 | Refurbished power dissipation system.

or loss of follower operation (e.g., manual mode or actuator failure).

2.2 | Analysis of Power Regulation

As explained in the previous section, the regulation of the dissipated power is achieved by changing the water level in the tank. This power can be calculated as:

$$P = 3\frac{V^2}{R} = 3\frac{V^2}{k\rho}l \tag{1}$$

where V is the line voltage, $R = k\rho/l$ is the value of each delta-connected resistance, l the length of the electrode immersed in the water, ρ is the water resistivity and k is a parameter that depends on the geometry of the electrodes. This dependence is linear in the control variable l, which simplifies regulation compared with approaches based on electrode spacing.

3 | Three-Phase Rheostat Configurations: Refurbished System

3.1 | Description

As a result of the repowering of the units, the original dump-load system, which had been operating satisfactorily, became undersized with respect to the new operating limits. In addition, its regulation principle is intrinsically slow, since power is controlled by changing the water level and therefore by moving a large water volume in a tank of substantial size. For this reason, a different regulation principle was pursued, based on controlling the electrode position rather than the water level, with the objective of increasing the regulation speed. However, the implemented refurbishment introduced critical issues that are analysed in the following sections.

In the implemented retrofit, the dump-load system consists of three insulating water tanks, one for each electrical phase, where the inlet and outlet water flows keep the water level constant (see Figure 3). In each tank there are two copper electrodes immersed in water: one is fixed at the bottom of the container, and one is

17521424, 2026, 1, Downloaded from https://ietresearch.onlinelibrary.wiley.com/doi/10.1049/rpg2.70312 by Fabio Freschi - Politecnico Di Torino Sist. Bibl Del Polit Di Torino , Wiley Online Library on [17/07/2026]. See the Terms and Conditions (https://onlinelibrary.wiley.com/terms-and-conditions) on Wiley Online Library for rules of use; OA articles are governed by the applicable Creative Commons License

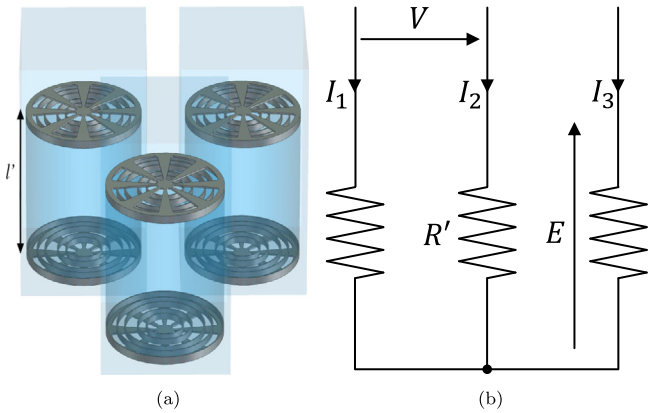


FIGURE 4 | (a) Sketch of the refurbished dump-load system, (b) equivalent circuit.

movable. The three single-phase loads are star-connected with the three fixed electrodes connected together to form the star point (see Figure 4). In the operating condition, the phase current flows from the movable to the fixed electrode through the water. Power regulation is achieved by varying the distance between the electrodes. In the implemented installation, l' varies between 0.3 and 0.9 m. The design target was a dissipated power of 8 MW per tank at rated voltage. The control system adjusts this distance to match the dump load with the instantaneous grid load so as not to create power transients.

3.2 | Analysis

From the electrical point of view, the three resistances of the rheostat can dissipate the power

$$P = 3\frac{E^2}{R'} = \frac{V^2}{k'\rho l'} \tag{2}$$

where $E = V/\sqrt{3}$ is the phase voltage, l' is the distance between the electrodes, ρ is the water resistivity and $R' = k'\rho l'$, with k' depending on the electrode geometry.

The maximum power dissipation is obtained when the distance between the electrodes is minimum. In principle, acting on the electrode position can provide a faster actuator than water level control. However, (2) shows that power depends on $1/l'$, which introduces a strong nonlinearity near the minimum distance.

4 | Testing of the Refurbished Solution

Before commissioning, the refurbished system was tested on site to characterize the electrical behavior of the electrode spacing regulation and to verify its operation up to rated voltage. The tests were conducted by progressively increasing the applied voltage up to 10 kV and, at each voltage level, by setting the electrode distance l' to a sequence of discrete positions within the admissible stroke. The total three-phase active power and the phase currents were recorded for each operating point.

TABLE 1 | Test points used to obtain Figure 5.

	1 kV		5 kV		10 kV	
l' (m)	P (MW)	R' (Ω)	P (MW)	R' (Ω)	P (MW)	R' (Ω)
0.30	0.135	7.392	3.935	6.352	—	—
0.35	—	—	—	—	18.844	5.306
0.40	0.099	10.075	—	—	16.406	6.095
0.50	0.080	12.442	2.165	11.547	11.279	8.865
0.60	0.067	14.918	—	—	8.601	11.626
0.70	0.058	17.183	1.532	16.309	7.011	14.262
0.80	0.050	19.637	—	—	5.897	16.956
0.90	0.044	22.552	1.158	21.575	5.054	19.785

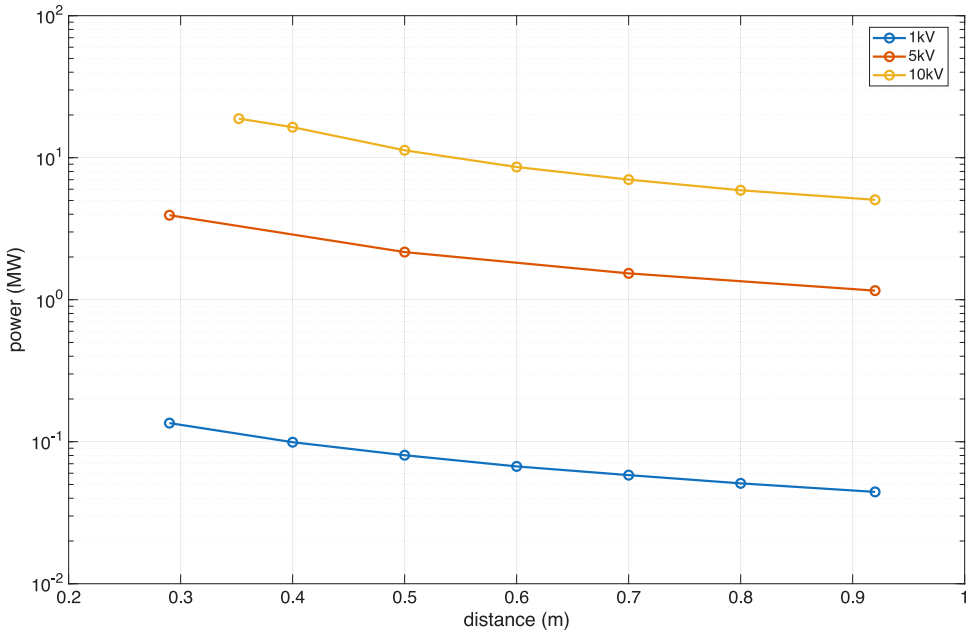
Figure 5a reports the measured total dissipated power versus l' at 1, 5 and 10 kV. The phase currents remained practically balanced throughout the campaign. The experimental curves confirm the inverse dependence of the power on l' predicted by Equation (2).

From the measured power values, the corresponding equivalent resistance was derived and plotted in Figure 5b. The resistance is not only proportional to l', but it also varies with the applied voltage. This behavior is consistent with thermal effects during the test: as the dissipated power increases, the water temperature rises and the resistivity decreases, leading to a lower apparent resistance at the same distance. The simulated resistance curve also shown in Figure 5b is included as a forward reference to the numerical analysis presented in Section 5.3, in order to compare measured and calculated resistance trends without duplicating the same plot.

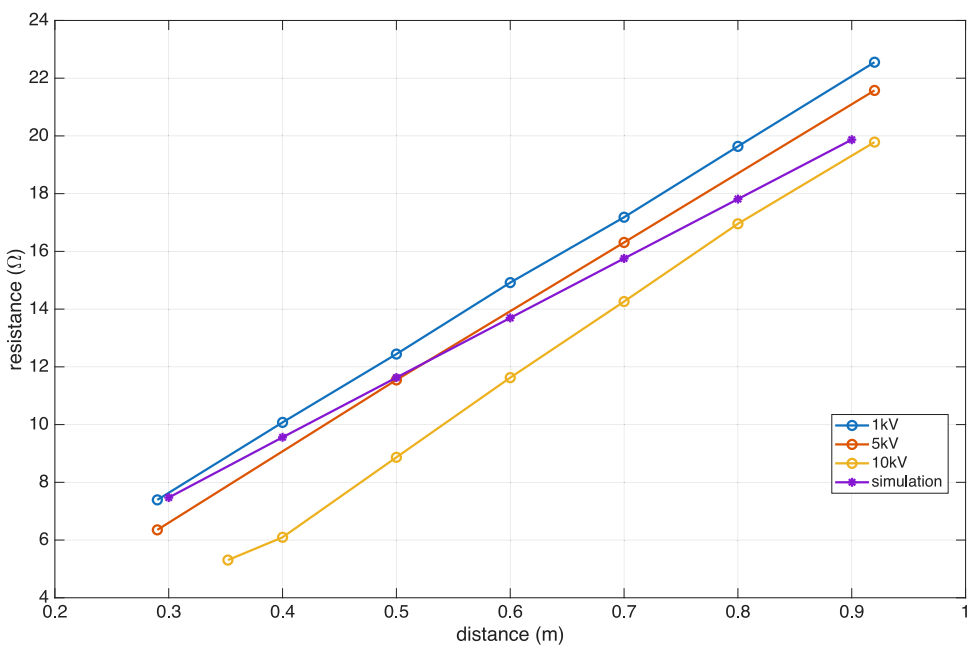
Table 1 reports the test points used to obtain Figure 5. For each voltage level and electrode distance l', the measured total three-phase active power P is listed together with the equivalent resistance R' derived from $R' = V^2/P$, where V is the line voltage.During the tests, two critical phenomena were observed at high voltage and high dissipated power. First, due to water overflow from the three tanks, visible phase-to-phase discharges occurred on the water surface between adjacent tanks, as shown in Figure 6a, which caused unintended trips of overcurrent protections. This behaviour is consistent with the fact that the overflowing water sheets can come into contact, or approach each other, while being at different potentials.

Second, approaching rated conditions, significant steam formation was observed, as shown in Figure 6b. This suggests the presence of local hot zones in the tank, which is consistent with a non-uniform thermal field and with recirculation patterns that can develop around the upper electrode, depending on the inlet layout and the resulting flow distribution. Following these observations, the supplier attributed the issues mainly to insufficient ventilation and water flow and proposed increasing tank dimensions and adding phase separators. However, since the working principle and the overflow arrangement remained unchanged, a deeper analysis was required to assess whether the observed phenomena were incidental or intrinsic to the adopted design, which motivates the numerical study presented in Section 5.

17521424, 2026, 1, Downloaded from https://ietresearch.onlinelibrary.wiley.com/doi/10.1049/rpg2.70312 by Fabio Freschi - Politecnico Di Torino Sist. Bibl Del Polit Di Torino , Wiley Online Library on [17/07/2026]. See the Terms and Conditions (https://onlinelibrary.wiley.com/terms-and-conditions) on Wiley Online Library for rules of use; OA articles are governed by the applicable Creative Commons License



(a)



(b)

FIGURE 5 | Testing of the refurbished solution at different voltage levels: (a) measured power versus electrode distance, (b) measured equivalent resistance versus electrode distance. The simulated curve in (b) refers to the numerical model described in Section 5.2 and discussed in Section 5.3.

5 | Electrical Analysis of the Refurbished System

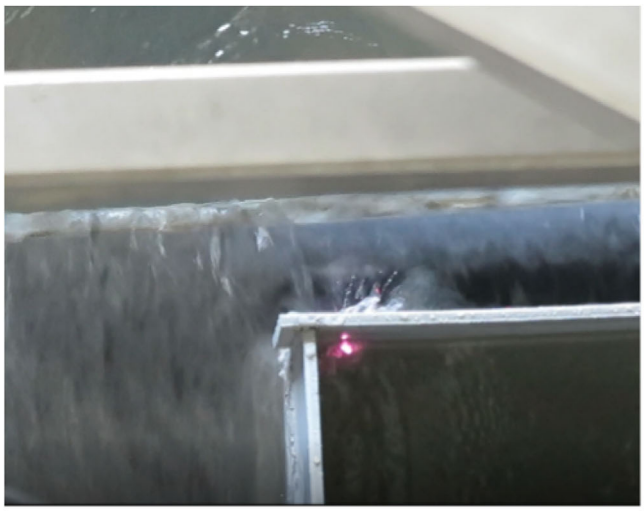
5.1 | Preliminaries

The structure studied consists of two electrodes and a tank filled with river water. The upper electrode position varies between 0.3 and 0.9 m with respect to the fixed lower electrode. Figure 7 shows the geometry and the detail of the electrodes. In the simulations, the water is described by a constant resistivity $\rho = 2960$ Ωcm at 15 °C, representative of freshwater rivers. All numerical results reported in the following sections are computed with an imposed electrode-to-electrode voltage equal to the operating phase voltage of 5.8 kV.

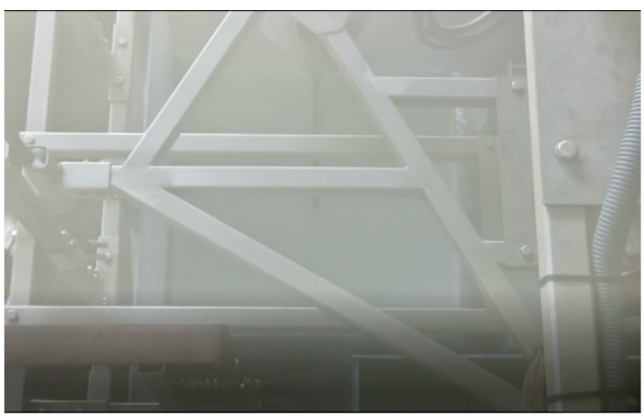
5.2 | Methodology and Modelling Assumptions

Two complementary numerical models were used to analyse the electric behavior of the electrodes. The first model solves the stationary current-flow problem in the conductive water

17521424, 2026, 1, Downloaded from https://ietresearch.onlinelibrary.wiley.com/doi/10.1049/rpg2.70312 by Fabio Freschi - Politecnico Di Torino Sist. Bibl Del Polit Di Torino , Wiley Online Library on [17/07/2026]. See the Terms and Conditions (https://onlinelibrary.wiley.com/terms-and-conditions) on Wiley Online Library for rules of use; OA articles are governed by the applicable Creative Commons License

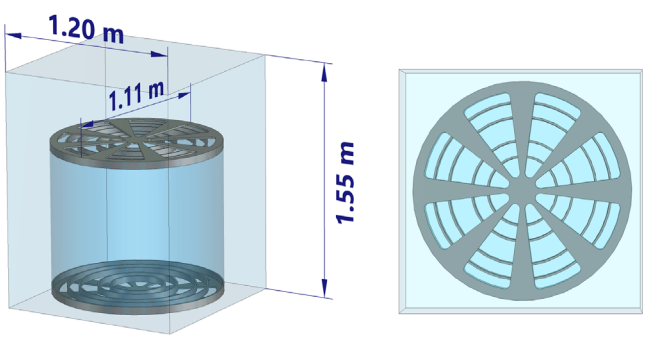


(a)



(b)

FIGURE 6 | (a) Electrical sparks between the spilling water and the tank of another phase, (b) steam formation at rated power.



(a) (b)

FIGURE 7 | Refurbished configuration: (a) geometry, (b) detail of the electrode (top view).

domain in order to compute the equivalent resistance, current density distribution and the resulting ohmic power dissipation. The second model solves the electrostatic problem to evaluate the electric field amplification driven by electrode geometry and to identify local overstress regions that may exceed the dielectric strength.

5.2.1 | Stationary Current-Flow Model

The water volume inside the tank is modelled as a linear, homogeneous and isotropic conductor with constant resistivity ρ. Electrodes are treated as perfect conductors at fixed electric potentials. Under steady conditions, the electric potential φ in the water satisfies

$$\nabla \cdot \left(\frac{1}{\rho} \nabla \varphi \right) = 0 \tag{3}$$

with boundary conditions $\varphi = \varphi_{\text{fix}}$ on the electrode surfaces, and insulating boundary conditions on the tank walls:

$$\vec{n} \cdot \vec{J} = 0 \tag{4}$$

The simulation boundary coincides with the inner tank surfaces, consistently with the assumption that the walls are insulating and no current leaves the water volume.

Once φ is computed, the current density is obtained from $\vec{J} = -\frac{1}{\rho} \nabla \varphi$. The total current associated with each electrode is computed by surface integration of $\vec{J} \cdot \vec{n}$, where $\vec{n}$ is the outward unit normal. The equivalent resistance is then derived from the imposed potential difference and the resulting current.

5.2.2 | Electrostatic Model

To assess the effect of electrode shape on the electric field, an electrostatic simulation is also performed with fixed electrode potentials. In the water domain, the electric potential satisfies

$$\nabla \cdot (\varepsilon \nabla \varphi) = 0 \tag{5}$$

where ε is the permittivity of the medium. The same Dirichlet boundary conditions $\varphi = \varphi_{\text{fix}}$ are imposed on electrode surfaces, while the tank walls are treated as electrically insulating boundaries. The electric field is then obtained as

$$\mathbf{E} = -\nabla \varphi. \tag{6}$$

This electrostatic model is used to locate local field amplification regions associated with sharp features and small radii of curvature. Although discharge inception and subsequent discharge dynamics cannot be predicted with a static model, the peak electric field provides a conservative indicator of local dielectric overstress.

5.2.3 | Software and Limitations

All simulations were performed with the commercial package CST Studio Suite [12]. The main limitations of the modelling approach are that temperature dependence of water resistivity is not included and water flow is not modelled. In practice, ρ varies seasonally and decreases with temperature, and local heating and recirculation can produce non-uniform resistivity fields. These effects can change the measured resistance and affect regulation,

17521424, 2026, 1, Downloaded from https://ietresearch.onlinelibrary.wiley.com/doi/10.1049/rpg2.70312 by Fabio Freschi - Politecnico Di Torino Sist. Bibl Del Polit Di Torino , Wiley Online Library on [17/07/2026]. See the Terms and Conditions (https://onlinelibrary.wiley.com/terms-and-conditions) on Wiley Online Library for rules of use; OA articles are governed by the applicable Creative Commons License

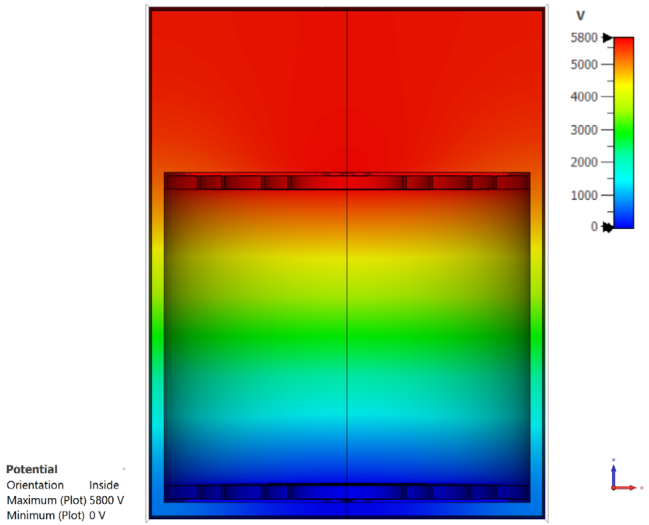


FIGURE 8 | Electrical potential (range 0–5.8 kV) with maximum electrode distance (0.9 m).

but they are outside the scope of the present models. Accordingly, the numerical results are used to interpret trends, identify geometric stress concentrations and define design constraints rather than to provide discharge-probability predictions.

5.3 | Electric Potential

An example of the analysis of the electric potential in the structure corresponding to the maximum distance between the electrodes is shown in Figure 8. It can be seen that the electric potential decreases almost linearly between the two electrodes in the case with the electrodes at maximum distance. The water volume above the upper electrode assumes the potential of that electrode. This result does not depend on tank size. Consequently, adjacent tanks operate at different phase potentials and the potential difference between tanks is the line voltage. When overflowing water sheets approach each other, the surface can be exposed to line-to-line voltage, which explains the discharges observed during testing. To mitigate this mechanism, the inter-tank distance and the overflow paths must be designed to prevent conductive water bridges between phases.

Figure 9 shows the current density distribution for electrodes at maximum distance. Since the system operates at an imposed voltage, the current (and therefore the current density) increases as the resistance decreases and the maximum electrical stress occurs at minimum electrode distance. In Figure 5b, the starred curve reports the simulated equivalent resistance as a function of electrode spacing, compared with the measured values. The calculated resistance curve lies between the measured values obtained at the different voltage levels of 1, 5 and 10 kV. The discrepancy between the numerical and experimental curves is consistent with the modelling assumptions introduced in Section 5.2. In the simulation, the water resistivity is assumed to be homogeneous and constant, whereas during the experimental tests the dissipated power caused water heating and therefore a reduction of resistivity. This effect becomes stronger at higher

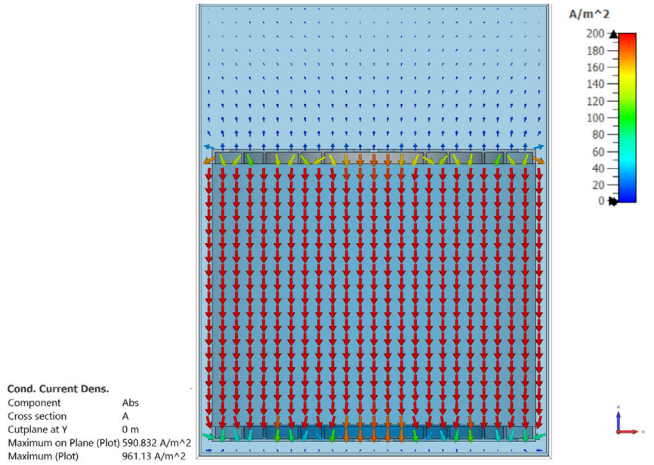


FIGURE 9 | Current density (range 0–200 A/m^2) with maximum electrode distance (0.9 m).

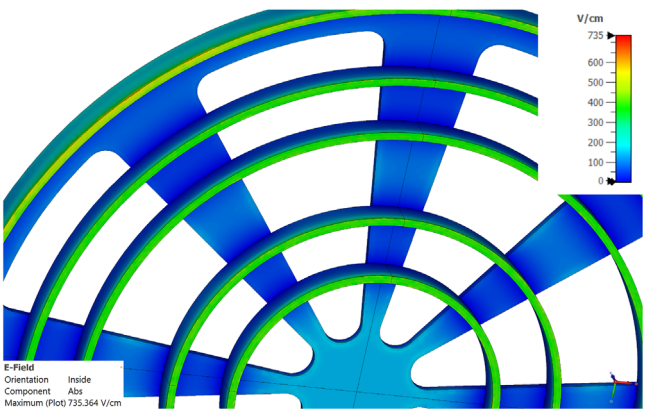


FIGURE 10 | Simulated electric field distribution on the upper electrode surface at a 30 cm spacing.

voltage and lower electrode spacing, where the dissipated power is larger. In addition, local heating and water recirculation may produce spatially non-uniform resistivity fields, which are not represented by the stationary electrical model. For this reason, the simulation is used to interpret the resistance trend associated with the electrode geometry, rather than to reproduce the complete thermohydraulic behaviour observed during the tests.

5.4 | Electric Field

Another critical point of the implemented retrofit is the geometry of the electrodes. The electrode base includes sharp-edged features where the electric field is intensified. Figure 10 shows the magnitude of the electric field on the surface of the top electrode for an electrode spacing of 30 cm. The electric field is maximum at the outermost fin, where it reaches 735 V/cm. This value locally exceeds the assumed design limit of 250 V/cm. Discharge inception cannot be predicted from this static analysis alone, because local overstress does not necessarily lead to a sustained discharge between electrodes. Nevertheless, the peak field exceeds the assumed design limit and must be treated as a critical design constraint.

17521424, 2026, 1, Downloaded from https://ietresearch.onlinelibrary.wiley.com/doi/10.1049/rpg2.70312 by Fabio Freschi - Politecnico Di Torino Sist. Bibl Del Polit Di Torino , Wiley Online Library on [17/07/2026]. See the Terms and Conditions (https://onlinelibrary.wiley.com/terms-and-conditions) on Wiley Online Library for rules of use; OA articles are governed by the applicable Creative Commons License

TABLE 2 | Design constraints derived from the case study.

Aspect	Constraint identified in the case study	Design implication
Electrode-spacing regulation	The dissipated power varies approximately as $1/l'$, making the system highly sensitive near the minimum electrode distance. For the analysed geometry, at $l' = 0.3$ m, a displacement of 1 cm corresponds to a power variation larger than 1 MW.	The sensitivity dP/dl', actuator accuracy, control margin and possible mechanical oscillations should be checked at the most demanding operating points.
Water resistivity and temperature	The measured resistance depends on the applied voltage, consistently with water heating and the associated reduction of resistivity during high-power tests.	Electrical sizing should include temperature-dependent resistivity and seasonal resistivity variation, rather than relying only on a fixed nominal value.
Thermal non-uniformity	Steam formation observed during testing indicates local hot zones and non-uniform temperature distribution.	Heat removal and flow distribution should be assessed to avoid local overheating near the electrodes.
Electrode geometry	The simulated electric field is locally amplified at sharp electrode features. At minimum spacing and rated voltage, the peak field exceeds the assumed design limit.	Electrode geometry should be rounded where possible, and the maximum local electric field should be verified using the full three-dimensional geometry.
Overflow paths	Overflowing water from adjacent tanks can be exposed to line-to-line voltage, explaining the phase-to-phase discharges observed during testing.	Overflow and drainage paths should prevent conductive water bridges or closely spaced water sheets between different phases.
Combined critical condition	Rated voltage and minimum electrode spacing combine maximum dissipated power, stronger heating, maximum electric-field stress and highest control sensitivity.	The design should be validated under the most severe combined operating condition, rather than by checking each constraint separately.

5.5 | Control System

From Equation (2) the dissipated power depends on $1/l'$, unlike the original solution in Equation (1) where power is proportional to the control variable. This nonlinearity makes regulation more difficult near maximum power, that is, close to the minimum electrode distance. In this region the sensitivity $\mathrm{d}P/\mathrm{d}l'$ is high and small positioning errors lead to large power variations. In fact, for $l' = 0.3$ m, a displacement of 1 cm corresponds to a power change larger than 1 MW.

5.6 | Summary of Design Constraints

The experimental observations and numerical results discussed above identify a set of design constraints that should be considered when refurbishing large water-rheostat dump loads. These constraints are summarized in Table 2. The table is not intended as a general design procedure, but as a synthesis of the critical points highlighted by the present case study.

6 | Conclusions

In this paper, the refurbishment of a large three-phase water-rheostat dump-load system for a grid-connected hydropower plant was analysed through field tests and three-dimensional electrical simulations. The investigated retrofit replaced immersion-depth regulation with electrode-spacing regulation, but the commissioned system did not achieve reliable operation at the specified power levels.

The analysis showed that the adopted configuration is affected by several coupled criticalities. First, the dissipated power is inversely proportional to the electrode spacing, making regulation highly sensitive near the minimum distance. For the present geometry, a displacement of 1 cm around $l' = 0.3$ m produces power variations exceeding 1 MW. Second, the electrode geometry produces strong local electric-field enhancement: at minimum spacing and rated voltage, the simulated peak field reaches 735 V/cm, exceeding the assumed design limit of 250 V/cm. Third, the overflow arrangement can expose water paths from adjacent tanks to line-to-line voltage, explaining the phase-to-phase discharges observed during testing. Finally, the measured resistance variation with voltage confirms the importance of thermal effects and temperature-dependent water resistivity, which must be considered in the design margins.

The case study shows that large water-rheostat dump loads cannot be validated only through simplified resistance-based sizing. Future refurbishments should jointly consider electrode geometry, hydraulic layout of overflow paths, thermal management, control sensitivity and seasonal variability of water resistivity. Although the numerical model used here is stationary and does not predict discharge inception or transient thermohydraulic behaviour, it provides useful evidence for identifying design constraints and interpreting the observed failure mechanisms.

17521424, 2026, 1, Downloaded from https://ietresearch.onlinelibrary.wiley.com/doi/10.1049/rpg2.70312 by Fabio Freschi - Politecnico Di Torino Sist. Bibl Del Polit Di Torino , Wiley Online Library on [17/07/2026]. See the Terms and Conditions (https://onlinelibrary.wiley.com/terms-and-conditions) on Wiley Online Library for rules of use; OA articles are governed by the applicable Creative Commons License

Author Contributions

Fabio Freschi: conceptualization, data curation, formal analysis, investigation, software, writing – original draft. **Marco Badami:** formal analysis, funding acquisition, project administration, supervision, writing – review & editing. **Michele Tartaglia:** conceptualization, supervision, validation, writing – original draft, writing – review & editing.

Acknowledgements

The authors thank Enel Green Power S.p.A. for providing access to project information and for the technical discussions.

Open access Funding provided by Politecnico di Torino within the CRUI-CARE agreement.

Funding

The authors have nothing to report.

Conflicts of Interest

The authors declare no conflicts of interest.

Data Availability Statement

Data sharing is not applicable to this article, as no datasets were generated or analysed during the current study.

References

1. F. Lemperiere, J. Vigny, and L. Deroo, "Most Dams Deserve Two Spillways," *International Journal on Hydropower & Dams* 25, no. 6 (2018).

2. C. Zhang, M. Yang, and J. Li, "Detailed Modelling and Parameters Optimisation Analysis on Governing System of Hydro-Turbine Generator Unit," *IET Generation, Transmission & Distribution* 12, no. 5 (2018): 1045–1051.

3. N. Ždankus, S. Vaikasas, and G. Sabas, "Protection of River Downstream of Hydropower Plant," *Journal of Applied Water Engineering and Research* 7, no. 1 (2019): 10–20.

4. R. Sebastián, "Application of a Battery Energy Storage for Frequency Regulation and Peak Shaving in a Wind Diesel Power System," *IET Generation, Transmission & Distribution* 10, no. 3 (2016): 764–770.

5. R. Singh, R. Dubey, and N. Sharma, "Review and Experimental Illustrations of Electronic Load Controller Used in Standalone Micro-Hydro Generating Plants," *Engineering Science and Technology, an International Journal* 21, no. 6 (2018): 1182–1192.

6. Alternative Energy Promotion Centre, *Reference Micro-Hydro Power Standard (1st Edition)* (Government of Nepal, 2014).

7. U. Lundin, P. Jonsson, and L. Facciolo, "Using Hydropower Turbine Discharge as a Complementary Spillway," *Journal of Applied Water Engineering and Research* 11, no. 1 (2023): 117–126.

8. U. Lundin and J. Bladh, "Demonstration of a Dynamic Braking System for Reduced Runaway Speed of Hydraulic Turbines," *Journal of Power and Energy Engineering* 5, no. 12 (2017): 1–13.

9. A. Peña-Pupo, R. González, L. Vega, J. Alfonso, and M. Armenteros, "Combined Method of Flow-Reduced Dump Load for Frequency Control of an Autonomous Micro-Hydropower," *Energies* 14, no. 23 (2021): 8135.

10. V. Patel, D. Patel, and S. Patel, "Technique to Reduce Dump Load in Isolated Hydro Power Plant by Load Frequency Control," *Journal for Research (J4R)* 2, no. 11 (2017): 3323–3326.

11. F. Freschi, M. Badami, and M. Tartaglia, "Three-Phase Dump Loads in Hydropower Plants: The Story of a Poor Design," in *2024 IEEE Industry Applications Society Annual Meeting (IAS)* (IEEE, 2024), 1–6.

12. CST Studio Suite, "Stationary Current Solver," 2024, accessed July 14, 2026, https://www.3ds.com/products/simulia/cst-studio-suite.

13. U.S. Environmental Protection Agency, "5.9 Conductivity – Water: Monitoring and Assessment," accessed July 14, 2026, https://archive.epa.gov/water/archive/web/html/vms59.html, accessed 2025.

14. M. Hayashi, "Temperature-Electrical Conductivity Relation of Water for Environmental Monitoring and Geophysical Data Inversion," *Environmental Monitoring and Assessment* 96 (2004): 119–128.

15. J. J. Barron and C. Ashton, "The Effect of Temperature on Conductivity Measurement," Reagecon Technical Paper TSP-07, 2005, accessed, July 14, 2026, https://www.reagecon.com/research-papers/temperature-effect-on-conductivity-measurement.

Appendix A: Electrical Resistivity of River Water

The electrical resistivity of river water depends on ionic content (salinity and dissolved minerals) and temperature. Freshwater rivers typically exhibit electrical conductivity values from about 50 to 1500 μS/cm, corresponding to resistivities in the range of 1 to 20 Ωm, depending on mineral content and temperature [13]. Mineral content affects the baseline conductivity through the concentration of dissolved ions (e.g., calcium, magnesium, sodium, chlorides); rivers flowing through mineral rich basins or influenced by anthropogenic inputs generally show higher conductivity, while mountain streams and pristine headwaters tend to have higher resistivity [13].

Conductivity also increases with temperature due to reduced viscosity and increased ionic mobility. Near 25 °C, a commonly used approximation is an increase of about 2% in conductivity per degree. Over the typical 0–30 °C range of natural waters, this dependence is often treated as approximately linear, and most measurements are corrected to a reference temperature of 25 °C [14, 15].

Seasonal variability is driven by both temperature and changes in water composition. In colder months, lower temperatures decrease conductivity; during warmer periods, conductivity increases due to both temperature and potential enrichment from baseflow or evaporation. Snowmelt and rainfall events can dilute ion concentrations, temporarily lowering conductivity in spring or early summer.

For the Po River (Italy), an extensive set of resistivity and temperature measurements collected between March 1958 and June 1960 illustrates the range of variability.

Figure A1 reports the historical original chart. For quantitative readability, the digitalized dataset is shown in Figure A2, reporting median, and interquartile range and min–max values as a function of temperature. The resistivity spans approximately 2500 to 5500 Ωcm (0.25–0.55 Ωm) and is inversely correlated with water temperature, which ranges from below 5 °C to over 25 °C.

17521424, 2026, 1, Downloaded from https://ietresearch.onlinelibrary.wiley.com/doi/10.1049/rpg2.70312 by Fabio Freschi - Politecnico Di Torino Sist. Bibl Del Polit Di Torino , Wiley Online Library on [17/07/2026]. See the Terms and Conditions (https://onlinelibrary.wiley.com/terms-and-conditions) on Wiley Online Library for rules of use; OA articles are governed by the applicable Creative Commons License

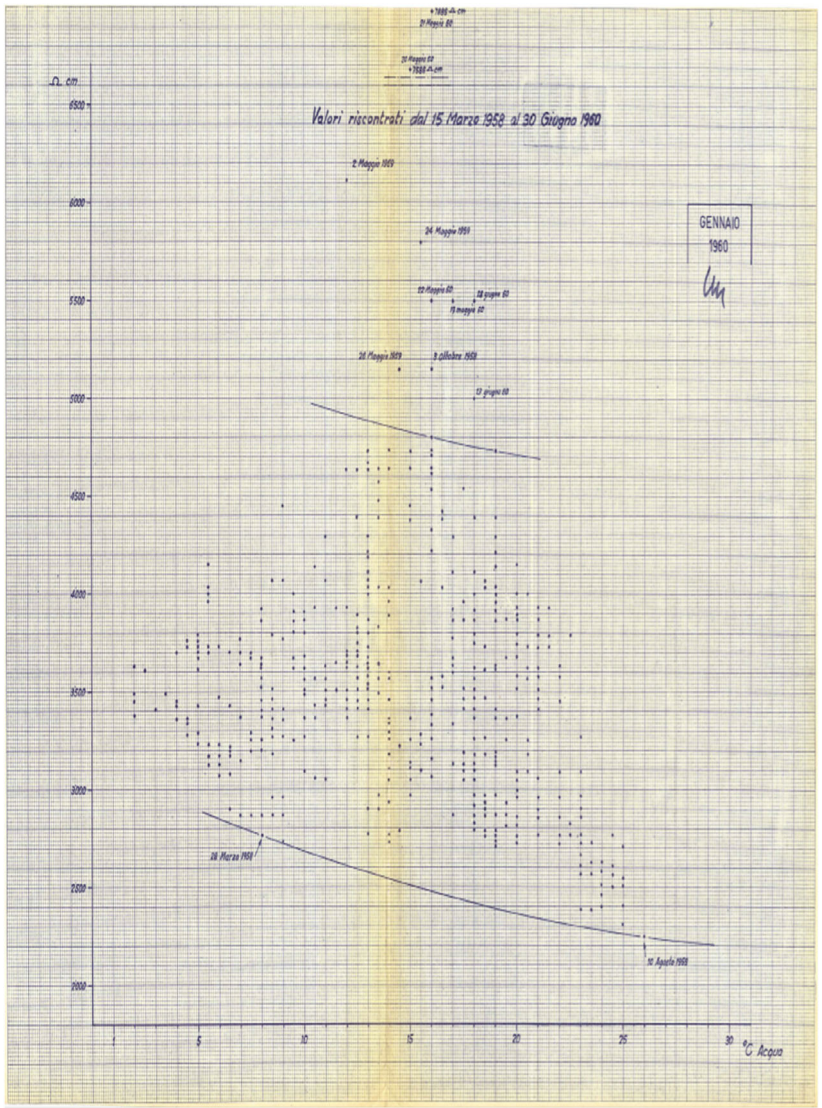


FIGURE A1 | Water temperature and resistivity measured between March 15, 1958 and June 30, 1960 (Courtesy of Enel Green Power S.p.A.).

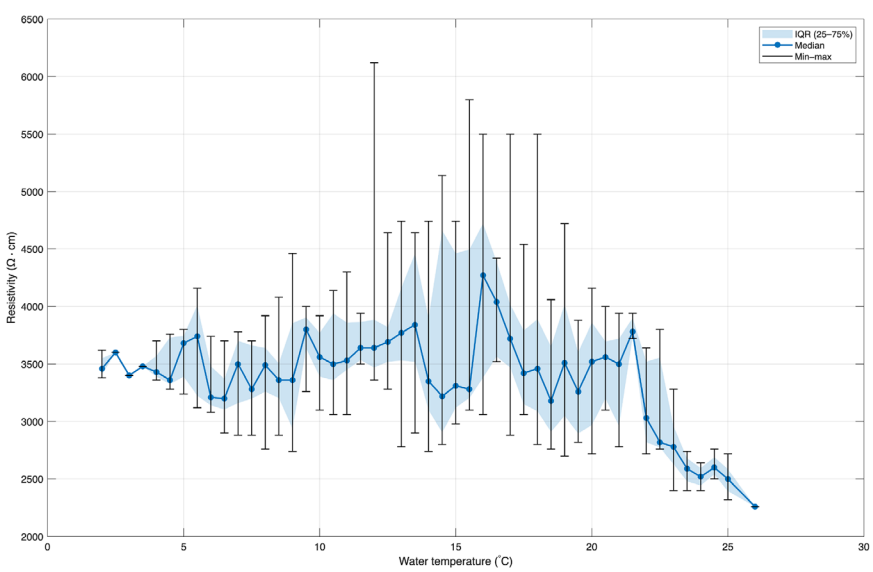


FIGURE A2 | Po River water resistivity as a function of temperature (digitized dataset from Figure A1). The median is shown with filled markers, the shaded band indicates the interquartile range (25% – 75%), and whiskers report the minimum and maximum values in each temperature interval.

17521424, 2026, 1, Downloaded from https://ietresearch.onlinelibrary.wiley.com/doi/10.1049/rpg2.70312 by Fabio Freschi - Politecnico Di Torino Sist. Bibl Del Polit Di Torino , Wiley Online Library on [17/07/2026]. See the Terms and Conditions (https://onlinelibrary.wiley.com/terms-and-conditions) on Wiley Online Library for rules of use; OA articles are governed by the applicable Creative Commons License